Bidirectional Soft Silicone Curvature Sensor Based on Off-Centered Embedded Fiber Bragg Grating

Jia Ge, Aneek Enrique James, Li Xu, Yue Chen, Ka-Wai Kwok, and Mable P. Fok, *Member, IEEE*

***Abstract*— A compact bidirectional soft curvature sensor is achieved by embedding a fiber Bragg grating (FBG) off-centered in a silicone sheet. The proposed approach is capable to distinguish both the bending curvatures and bending directions through wavelength shift measurement of the FBG. Based on the pure bending model, the relationship between the FBG embedded position and the sensor sensitivity is studied and verified experimentally. Real-time curvature measurement of both positive and negative bending directions is experimentally achieved. The curvature sensor has a consistent performance and the results are highly repeatable with small variances. A linear relationship between applied curvature and FBG wavelength shift is obtained, with a large measurement range of up to ±80 m^{-1} curvature.**

***Index Terms*— Soft robotics sensor, fiber optics sensor, fiber Bragg grating, bidirectional curvature sensor.**

I. Introduction

CURVATURE sensors have a wide array of applications, including structural health monitoring in civil engineering, motion detection of wearable devices for biomedical purposes [1], as well as real-time sensing of soft robotic configuration [2]. Fiber optic sensor research has been booming over the last decade [3]–[7] due to its unique advantages over conventional electronic sensors, including its light weight and tiny size, low transmission loss for long distance measurement, instant response, immune to electromagnetic interference, chemically inert, and nontoxic, i.e. not harmful to human body as a *in vivo* sensor. The unique properties of fiber optic sensor make it a good candidate for soft robotics and biomedical application. To date, several schemes of fiber optics based curvature sensors have been investigated, including the use of interferometric structure for phase modulation [8], specialty fibers with unique structures [9], and various types of fiber gratings [10]–[13]. Although the interferometric structure and specialty fiber schemes are usually having a higher sensitivity than most other alternatives, they are not favorable for implementation due to the structure complexity and high fabrication cost.

Manuscript received May 12, 2016; revised June 20, 2016; accepted July 11, 2016. Date of publication July 13, 2016; date of current version September 13, 2016. This work was supported by the National Science Foundation under Grant CMMI 1400100.

J. Ge, A. E. James, L. Xu, and M. P. Fok are with the Lightwave and Microwave Photonics Laboratory, The University of Georgia, Athens, GA 30605 USA (e-mail: jiage@uga.edu; aejames@uga.edu; lilyxu@uga.edu; mfok@uga.edu).

Y. Chen is with the Medical Robotics Laboratory, The University of Georgia, Athens, GA 30605 USA (e-mail: ychen@uga.edu).

K.-W. Kwok is with the Department of Mechanical Engineering, The University of Hong Kong, Hong Kong (e-mail: kwokkw@hku.hk).

Color versions of one or more of the figures in this letter are available online at http://ieeexplore.ieee.org.

Digital Object Identifier 10.1109/LPT.2016.2590984

On the other hand, the fabrication process of fiber grating is simple and mature, which has been well developed and widely used. The period of the grating determines the reflected wavelength, which is sensitive to the applied force and bending, resulting in a change in reflected wavelength. Examples of fiber Bragg grating (FBG) based curvature sensors include using a tilted FBG [10], splicing a standard FBG with a multimode fiber [11], using multi-FBG structure for respiration movement monitoring [12], and a static bending sensor based on FBG embedded shape memory polymers [13]. The above approaches either have a limited measurement range between ±2 cm^{-1} to 15.5 m^{-1} due to the requirement of strong glues for fixing the FBG, or incapable of distinguishing bending directions and real-time measurement due to the complex (de)formation processes. These limitations in curvature sensor hinder their usage in many applications. To enable reliable and high fidelity curvature sensing, real-time soft curvature sensors capable of measuring both bending directions and bending curvatures with a large sensing range is highly desired.

In this letter, we demonstrate a soft curvature sensor with compact and glue-free design, as well as a large measurement range of 80 m^{-1}. The sensor consists of a standard FBG that is embedded inside a silicone rubber sheet at an off-centered position and the embedded depth is precisely controlled by 3D printing technology. Unlike conventional FBG based curvature sensors that the grating is glued on the surface of the sensor, the FBG in our approach is embedded precisely at a particular designed position inside the silicone sheet without using any adhesives, such that the FBG is well protected by the silicone rubber and sensor sensitivity is adjustable by controlling the embedded depth. Detailed analysis of the sensor mechanical model and working principle are presented in Section II. Four sets of sensor samples with identical FBGs that are embedded at different depths of the silicone sheet are investigated. The proposed sensor is very soft and its curvature follows the contour of the object for testing in real-time. Furthermore, it is capable of distinguishing curvatures in both bending directions with sensitivity up to 1.64 pm/m^{-1}. Curvature measurement range of up to 80 m^{-1} is obtained with consistent and repeatable performance, which is significantly larger than other existing approaches. The large measurement range and the ability to distinguish bending directions in real-time make the proposed sensor to be a promising candidate for soft robotics, *in vivo* procedures, and surface sensing.

II. Fabrication and Principle

A. Embedding FBG Into Silicone Sheet

To achieve real-time sensing with a large measurement range, the adopted sensor material must be soft enough to be bend freely with the testing objects, while the FBG must be fixed to the sensor material. The use of strong glues for fixing

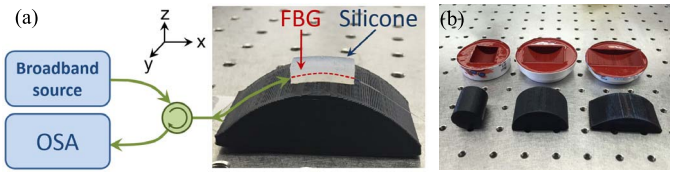

Fig. 1. (a) Bidirectional soft silicone curvature sensor and the measurement setup. (b) Testing objects with different positive/negative bending curvatures up to 80 m^{-1}.

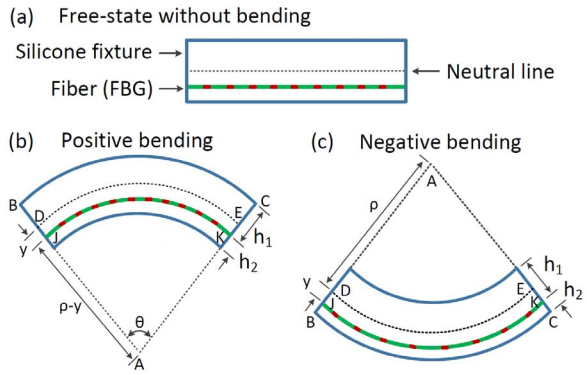

Fig. 2. Operating principle of the FBG based bidirectional curvature sensor. (a) Free-state of the curvature sensor, the dashed black line is the neutral line of the sensor, green line is referring to the fiber and red dash line is the FBG. (b) Positive bending situation. (c) Negative bending situation.

the FBG is not desired since the physical property of both the sensor material and the FBG will be affected. Here, we propose the use of silicone as the sensor material as well as the material to fix the FBG in position. Figure 1(a) shows the proposed soft silicone curvature sensor as well as the measuring setup, where FBG is embedded inside a flat silicone sheet and is fixed very well without using any adhesive. The FBG is centered along the y-direction in the silicone sheet coordinate but offset from the center in the z-direction. The cross-section view of the sensor, shown in Fig. 2, indicates the silicone sheet acts as a solid media tightly interacting with the FBG under constant curvature deformation. Due to the soft property of the silicone sheet, it can be placed onto and complied with the tested objects along the exact same curvature profiles.

In this study, Ecoflex® GEL from Smooth-On Inc. [14] is adopted as the silicone material. This soft material is elastic and capable of being stretched many times and still rebounds to its original shape without any distortion. In addition, it is certified for biological evaluation of medical devices with irritation and skin sensitization tests. The fabrication process mainly consists of four steps, which are (1) mold design and 3D printing, (2) lower layer molding, (3) FBG integration and upper layer molding, (4) de-molding. In step (1), the mold of silicone rubber is fabricated through a 3D printer with a fabrication precision of 50 μm. Then in step (2), equal amount of Ecoflex solutions are mixed and poured into the mold to fabricate the lower layer of the curvature sensor with a thickness of h_2, as illustrated in Fig. 2. In step (3), a FBG is placed on the top of the lower layer, leveled, and is fixed at the two end of the FBG, such that it is flat and parallel to the surface of the mold. Then, the mixed silicone solution is poured into the mold to create the upper layer with a thickness of h_1. The silicone rubber is cured for 4 hours at a temperature of 25 °C. Finally, the curvature sensor is demolded after the upper layer is cured. In the test experiment, the overall dimensions of the sensor are 5 mm in height (h_1+h_2), 10 mm in width and 20 mm in length. The FBG used in the sensor is a standard FBG fabricated by UV written technique, which has uniform grating pitches, an overall grating length of 20 mm, side-mode suppression of 26 dB, and a reflectivity of 92.9%. In the test the thicknesses of upper layer (h_1) and lower layer (h_2) are set ranging from 4.5:0.5 to 2.5:2.5 (mm) in five sensor samples, such that the relation between the FBG offset position and sensor sensitivity can be investigated.

B. Measuring Principle

When the FBG embedded sensor is placed on top of a curved surface, bending occurs on both the silicone sheet and the embedded FBG. Two bending directions, +z and −z, can be observed on a curved surface, that positive bending is defined as when the FBG is closer to the inner arc of the bend, while negative bending is defined when the FBG is further away from the inner arc, as illustrated in Fig. 2(b) and 2(c). The reflected wavelength λ_B of the FBG is determined by its grating period, which can be written as:

$$\lambda_B = 2n_e \cdot \Lambda \tag{1}$$

where n_e and Λ are the effective refractive index and the grating period, respectively. The bending effect of the embedded FBG will either stretch or compress the grating period, resulting in a change in the reflected wavelength. Stretched gratings will have a longer grating period Λ causing the reflection peak λ_B shift to longer wavelengths (red shift), while compressed gratings will result in a shift to shorter wavelengths (blue shift).

Different from most of the FBG based curvature sensors where the gratings are glued at the surface of the sensor, the FBG in our approach is embedded at an offset position from the neutral line (indicated by the dashed line D-E in Fig. 2(b)). As a result, positive bending and negative bending have different effects on the grating period. The distance from the FBG to the outer arc and inner arc of the silicone sheet is defined as h_1 and h_2, respectively, as shown in Fig. 2(b) and 2(c). The design and analysis of our sensor are based on the pure bending model [15], which is a classic and widely adopted model in mechanical engineering for describing a bending moment. Thus, when the sensor is bent as illustrated in Fig. 2(b), the relationship between the length of the neutral line, bending radius, and the bending angle is governed by

$$L_{DE} = \rho \cdot \theta \tag{2}$$

where L_{DE} is the length of the neutral line of the silicone sheet, which is always a constant value under all curvatures according to pure bending model [15]. ρ and θ are the radius and central angle at the neutral line, respectively. In general, the curvature C and the bending radius has a reciprocal relationship, as

$$C = 1/\rho = \theta/L_{DE} \tag{3}$$

Since the FBG is very thin and is embedded inside the silicone sheet, the FBG and the silicone sheet can be treated as a uniform object undergoing the same bending. That is to say, the FBG is compressed during positive bending, while it is stretched during negative bending. The offset location (y) of the FBG results in slightly modification in the bending radius

and is represented by $\rho \pm y$, depending on if it is a positive or negative bending. Then, we can obtain the length of FBG (L_{JK}) under an applied curvature, as

$$L_{JK} = (\rho \pm y) \cdot \theta \tag{4}$$

$$\Delta L_{FBG} = L_{DE} - L_{JK} = \pm\theta \cdot y \tag{5}$$

$$y = h_1 - (h_1 + h_2)/2 \tag{6}$$

where y is the distance between the neutral line and the FBG, and is fixed for a certain design. The bending induced change in the FBG length is derived as Eq. (5), which means that the grating period is changed proportionally to the bending angle θ (or curvature C), thus, a wavelength shift of the Bragg wavelength is resulted according to Eq. (1) and Eq. (3), and can be described as

$$\Delta\lambda_B \propto \pm n_e \cdot C \cdot L_{DE} \cdot (h_1 - h_2) \tag{7}$$

In Eq. (7), L_{DE} is a constant value in the pure bending model, and h_1 and h_2 are predetermined during the fabrication process for each sensor. Consequently, the amount of the wavelength shift is solely governed by the measured curvature C. It is worth noticing that the sensor is designed to be thin and small, and is for measuring relative large curvatures (i.e. $\rho \gg y$). However, when the measured curvature is comparable to the sensor thickness, then C should be considered as

$$C = 1/(\rho \pm y) \tag{8}$$

and a small measurement difference between positive and negative bending will be resulted. This explains the discrepancy that will be seeing in the measured results in Fig. 4 and Fig. 5 when the offset (y) is large. During the design of the curvature sensor, the value of h_1-h_2 provides the feasibility to adjust the sensor sensitivity as well as the capability to measure bi-direction bending. Showing in Fig. 2(b) is a situation when the FBG is bent closer to the inner arc, i.e. h_1-h_2 is a positive value (positive bending), a compression of the FBG is obtained because $L_{DE} > L_{JK}$. As a result, a blue shift of the Bragg wavelength is obtained from the reflection spectrum. On the contrary, when the sensor has a negative bending as shown in Fig. 2(c), i.e. h_1-h_2 is a negative value, stretching of the FBG and a red shift is observed. Finally, by measuring the direction and the amount of the wavelength shift, both the bending directions and curvatures can be determined. Notice that if the FBG is positioned at the neutral line of the sensor, i.e. h_1 equals h_2, L_{DE} is always a constant under pure bending, meaning that $\Delta\lambda_B$ is always 0. The sensor's sensitivity is governed by the amount of wavelength shift under certain amount of bending, which is determined by the h_1-h_2 value according to Eq. (7). Thus, by adjusting the FBG embedded depth during the fabrication process, different sensitivities can be resulted. The measurement setup (shown in Fig. 1(a)) consists of a broadband light source, an optical circulator, and an optical spectrum analyzer. Two sets of testing objects, a total of 15 pieces (including a flat surface) with 8 different bending curvatures from 0 to 80 m^{-1} are used. The concave (red) and convex (black) testing objects, shown in Fig. 1(b), are used for negative and positive bending measurement respectively.

III. Results and Discussion

Figure 3 shows the measured reflection spectra of the proposed FBG embedded silicone curvature sensor in response to different bending curvatures. The tested sensor has a 20 mm FBG inside, with embedded h_1:h_2 values of 4:1 (mm). The sensor is put on the top of the testing objects with bending curvatures from 0 to 80 m^{-1} as shown in Fig. 1(b). Measured spectra resulting from positive bending and negative bending are shown in Fig. 3(a) and 3(b), respectively. As shown in the positive bending situation in Fig. 3(a), FBG reflection peak gradually shifts to the shorter wavelength direction as the curvature increases, with a total wavelength shift of 0.091 nm under a curvature of 80 m^{-1}. During negative bending situation, the peak shifts to the longer wavelength direction, with a total wavelength shift of 0.095 nm under the same curvature. The measurement sensitivity is 1.1375 pm/m^{-1} for positive bending and 1.1875 pm/m^{-1} for negative bending. The experiment agrees with the theoretical predictions that the direction of the wavelength shift in response to positive bending and negative bending are opposite, and can be used to distinguish the bending directions. The profile of the FBG reflection peaks, as well as the property of the silicone material, are well maintained throughout the bending from 0 to $\pm$80 m^{-1}. A further increase in measured curvature to above $\pm$80 m^{-1} will cause over bending of the sensor and unequal changes in grating period, which will result in chirping of the FBG as well as potential damage of the sensor. The response of the sensor is instantaneous and can measure dynamic movements in real-time without the need of molding/formation process. Due to the small amount of wavelength shift, a large number of FBG sensors at different wavelength can be cascaded in a single fiber for multi-point curvature sensing or shape sensing. An interrogator that consists of two single wavelength light source and a photodetector can be used with the proposed sensor to support fast measurement [16].

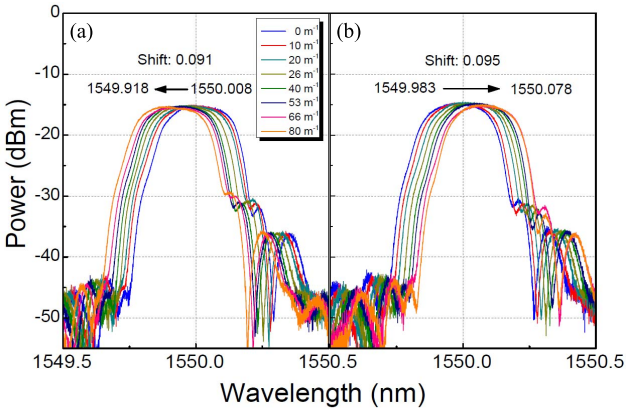

Fig. 3. Measured FBG reflection spectra of the curvature sensor under different bending curvatures, with embedded h_1:h_2 values of 4:1 (mm). (a) Positive bending. (b) Negative bending.

We also studied the relationship between the sensor sensitivity and FBG embedded depth by fabricating four testing sensors with different embedded depths (h_2) from 0.5 mm to 2.0 mm. Figure 4 shows the measured FBG reflection peak shifts of the four sensors under both positive and negative bending curvatures from 0 to 80 m^{-1}. Four identical FBGs are used, with the same reflection wavelength, initial grating period, grating length (20 mm) and overall sensor size. The h_1:h_2 values for the #1 to #4 sensors are 4.5:0.5, 4:1, 3.5:1.5 and 3:2 (mm), respectively. As shown, positive bending results of all the four sensors show blue

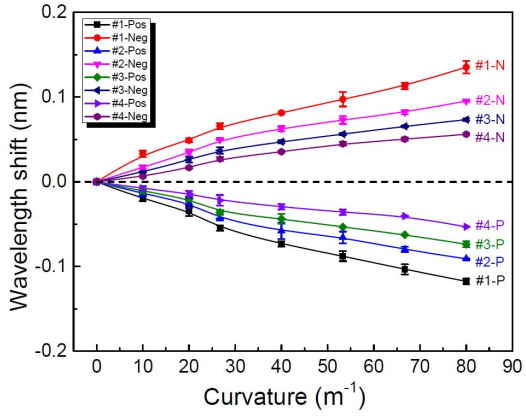

Fig. 4. Measured reflection peak shifts of 4 tested sensors under different amount of curvatures, with different FBG embedded depths. h_1:h_2 values for #1 to #4 sensors are 4.5:0.5, 4:1, 3.5:1.5 and 3:2 (mm), respectively.

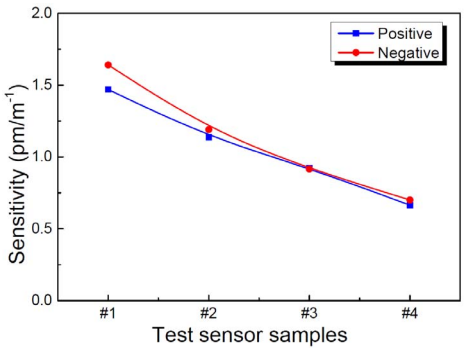

Fig. 5. Comparison of the sensor sensitivities with different FBG embedded depths, for both positive and negative bending.

wavelength shifts, corresponds to compressions in grating period; while negative bendings result in red wavelength shifts, indicating stretching in grating period. Under the same amount of bending curvature, the amount of wavelength shift is governed by the FBG embedded depth, i.e. h_1-h_2 value, which in turn governs the sensitivity. Figure 5 shows the calculated sensitivities of the four FBG sensor samples with different embedded depths. As shown, similar sensitivities of positive and negative bending are recorded at the same h_1-h_2 values, and the sensor sensitivities increase as the h_1-h_2 values increase. A largest bending sensitivity of 1.64 pm/m^{-1} is achieved with an embedded depth of 0.5 mm. All the measurements are repeated five times and corresponding error bars are shown in Fig. 4 to indicate the variances. The sensors have good accuracy and consistency over different measurements. A control experiment is also performed that a same FBG is embedded at the neutral line of the silicone sheet, with $h_1 = h_2$, while all the fabrication and experiment parameters are set to be the same as before. In this test, there is no significant wavelength shift for both positive and negative bending. This particular structure is incapable to tell the direction of bending, since the compression or stretching of the gratings are not significant when bending is applied, as predicted in the pure bending model in Eq. (7). It is worth noticing that to properly protect and fix the FBG inside the silicone sheet for measuring large bending curvatures, a minium protection thickness of 0.5 mm between the FBG and the sensor surface is needed.

IV. Summary

A bidirectional soft curvature sensor based on embedding a FBG in a flexible silicone sheet is demonstrated. Unlike conventional FBG curvature sensor, the proposed sensor has the FBG being embedded offset from the neutral line of the silicone sheet without using any adhesives. The soft silicone sensor does not require a formation time during measurement, enabling real-time curvature sensing. A large curvature measurement range of 80 m^{-1} is obtained for both positive and negative bending. The relationship between FBG embedded depth and sensor sensitivity is studied through the pure bending model and verified experimentally. The amount of wavelength shift has a linear relationship with the bending curvature for various embedded depths. A design with multiple FBGs is anticipated for sensing shapes with rather complex morphology. Such continuous FBG-based sensing technique makes it possible to acquire high-fidelity geometric details of many non-rigid objects deformed by the dynamic and unstructured environment, in particular for real-time structural monitoring in civil engineering, robotic control in mechanical engineering, and *in vivo* procedure in biomedical applications.

References

[1] A. T. Asbeck, S. M. M. De Rossi, I. Galiana, Y. Ding, and C. J. Walsh, "Stronger, smarter, softer: Next-generation wearable robots," *IEEE Robot. Autom. Mag.*, vol. 21, no. 4, pp. 22–33, Dec. 2014.

[2] C. Majidi, R. Kramer, and R. J. Wood, "A non-differential elastomer curvature sensor for softer-than-skin electronics," *Smart Mater. Struct.*, vol. 20, no. 10, p. 105017, Oct. 2011.

[3] A. Kersey *et al.*, "Fiber grating sensors," *J. Lightw. Technol.*, vol. 15, no. 8, pp. 1442–1463, Aug. 1997.

[4] J. Ge, H. Feng, Y. Chen, Z. T. H. Tse, and M. P. Fok, "Spiral-structured fiber Bragg grating for contact force sensing through direct power measurement," *Opt. Exp.*, vol. 22, no. 9, pp. 10439–10445, May 2014.

[5] H. Chen, F. Tian, J. Chi, J. Kanka, and H. Du, "Advantage of multi-mode sapphire optical fiber for evanescent-field SERS sensing," *Opt. Lett.*, vol. 39, no. 20, pp. 5822–5825, Oct. 2014.

[6] L. Xu, M. I. Miller, J. Ge, K. R. Nilsson, Z. T. H. Tse, and M. P. Fok, "Temperature-insensitive fiber-optic contact force sensor for steerable catheters," *IEEE Sensors J.*, vol. 16, no. 12, pp. 4771–4775, Jun. 2016.

[7] Y. Chen, J. Ge, K.-W. Kwok, K. R. Nilsson, M. P. Fok, and Z. T. H. Tse, "MRI-conditional catheter sensor for contact force and temperature monitoring during cardiac electrophysiological procedures," *J. Cardiovascular Magn. Reson.*, vol. 16, no. 1, pp. 150–152, Jan. 2014.

[8] W. Shin, Y. L. Lee, B.-A. Yu, Y.-C. Noh, and T. J. Ahn, "Highly sensitive strain and bending sensor based on in-line fiber Mach–Zehnder interferometer in solid core large mode area photonic crystal fiber," *Opt. Commun.*, vol. 283, no. 10, pp. 2097–2101, May 2010.

[9] D. Monzon-Hernandez, A. Martinez-Rios, I. Torres-Gomez, and G. Salceda-Delgado, "Compact optical fiber curvature sensor based on concatenating two tapers," *Opt. Lett.*, vol. 36, no. 22, pp. 4380–4382, Nov. 2011.

[10] C. Caucheteur, K. Chah, F. Lhommé, M. Blondel, and P. Mégret, "Simultaneous bend and temperature sensor using tilted FBG," *Proc. SPIE*, vol. 5855, pp. 707–710, May 2005.

[11] W. Zhou, Y. Zhou, X. Dong, L. Shao, J. Cheng, and J. Albert, "Fiber-optic curvature sensor based on cladding-mode Bragg grating excited by fiber multimode interferometer," *IEEE Photon. J.*, vol. 4, no. 3, pp. 1051–1057, Jun. 2012.

[12] T. Allsop *et al.*, "Respiratory function monitoring using a real-time three-dimensional fiber-optic shaping sensing scheme based upon fiber Bragg gratings," *J. Biomed. Opt.*, vol. 17, no. 11, p. 117001, Nov. 2012.

[13] P. Li, Z. Yan, K. Zhou, L. Zhang, and J. Leng, "Monitoring static shape memory polymers using a fiber Bragg grating as a vector-bending sensor," *Opt. Eng.*, vol. 52, no. 1, p. 014401, Jan. 2013.

[14] Smooth-On, Inc. [Online]. Available: http://www.smooth-on.com/

[15] A. P. Boresi and R. J. Schmidt, *Advanced Mechanics of Materials*, vol. 5. New York, NY, USA: Wiley, 1993, pp. 6–7.

[16] M. Kreuzer, *Strain Measurement With Fiber Bragg Grating Sensors*. Darmstadt, Germany: HBM Test and Measurement, 2006.